INTERNATIONAL JOURNAL OF HYDROGEN ENERGY 48 (2023) 25398–25409

Available online at www.sciencedirect.com

ScienceDirect

journal homepage: www.elsevier.com/locate/he

# Development of selective Pd–Ag membranes on porous metal filters

S. Agnolin [a], F. Apostolo [a], L. Di Felice [a], J. Melendez Rey [b], A. Pacheko Tanaka [c], M. Llosa Tanco [c], F. Gallucci [a,d,*]

[a] Inorganic Membranes and Membrane Reactors, Sustainable Process Engineering, Department of Chemical Engineering and Chemistry, Eindhoven University of Technology, De Rondom 70, Eindhoven, 5612 AP, the Netherlands

[b] $H_2$Site, Bilbao, Spain

[c] TECNALIA, Basque Research and Technology Alliance (BRTA), Mikeletegi Pasealekua 2, 20009, Donostia, San Sebastian, Spain

[d] Eindhoven Institute for Renewable Energy Systems (EIRES), Eindhoven University of Technology, PO Box 513, Eindhoven 5600 MB, the Netherlands

## HIGHLIGHTS

- A method to fill the pores of Hastelloy filters via aspiration of α-$Al_2O_3$ water suspension has been developed.
- The effect of α-$Al_2O_3$ particle size on the surface quality has been studied with a statistical method.
- The asymmetrical filling method can reduce the average pore size of the filters from 1.1 μm up to 200 nm.
- A boehmite-based layer is used to change the surface quality and as interdiffusion barrier.
- A highly $H_2$-selective Pd–Ag membrane (~40 000) has been obtained on the asymmetrically filled support.

## GRAPHICAL ABSTRACT

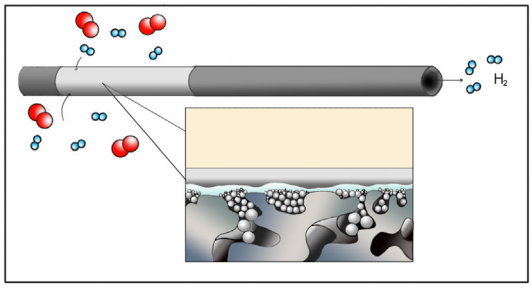


## ARTICLE INFO

*Article history:*
Received 11 February 2023
Received in revised form
10 March 2023

## ABSTRACT

Metallic supports with sufficient surface quality to achieve highly selective thin Pd–Ag membranes require specific pre-treatments, are not readily available on the market and are generally very expensive. To reduce costs, rough and large media grade Hastelloy X filters have been acquired and pre-treated via polishing and chemical etching. The loss in gas permeance given by the polishing treatment proved fully recovered after chemical

* *Corresponding author*. Inorganic Membranes and Membrane Reactors, Sustainable Process Engineering, Department of Chemical Engineering and Chemistry, Eindhoven University of Technology, De Rondom 70, Eindhoven, 5612 AP, the Netherlands.
E-mail address: f.gallucci@tue.nl (F. Gallucci).

https://doi.org/10.1016/j.ijhydene.2023.03.306

Accepted 20 March 2023
Available online 5 April 2023

*Keywords:*
Surface modification
Metallic membranes
Hydrogen separation
Pd membranes
Metallic supports

etching. A method to fill the large pores of the filters via aspiration of $\alpha$-$Al_2O_3$ water-powder suspension has been applied and characterized via imaging of the filled pores, inferential statistics, and capillary flow porometry measurements. The most suitable filler particle size for pore size distribution reduction has been identified as 18 μm, while a 5 μm filler proved optimal for further pore morphology improvement. The wide pore size distribution of the filters has thus been reduced up to 200 nm by filling with $\alpha$-$Al_2O_3$ particles of decreasing size, similarly to the ceramic supports used for thin Pd–Ag membranes deposition. A boehmite based interdiffusion barrier has been deposited, achieving further surface roughness reduction. A highly $H_2$ selective membrane has been obtained via simultaneous Pd–Ag plating on the pre-treated filter.



## Introduction

Pd based membranes are well-known for their unique solution-diffusion $H_2$ transport mechanism, which makes them the heart of membrane reactors (MRs) for in-situ selective hydrogen removal [1–3]. MRs have proven themselves as a promising alternative to conventional methane steam reformers by integrating both reaction and separation in a single unit and thus avoiding the purification steps required by a conventional process [4–6]. The introduction of membranes in the reaction environment promotes in fact the continuous removal of $H_2$, resulting in equilibrium shift towards the $H_2$ production reaction owing to the Le Chatelier's principle. In this way, the process operating temperature is reduced, increasing overall energy efficiency and reducing operational costs [7–9].

As core of this intensification technology, Pd-based membranes have been subjected to optimization studies, mostly both in terms of their $H_2$ perm-selectivity performance and their suitability for integration in the reaction environment [10–12]. In particular, thin Pd films (<10 μm) have been successfully deposited on tubular ceramic supports [13,14]. The deposition of Pd on an appropriate support allows in fact to reach outstanding $H_2$ perm-selectivity while ensuring mechanical stability of the thin films [12,15,16]. Asymmetric ceramic tubular supports prove in fact suitable for the electroless deposition of a thin and defect-free Pd-based layer thanks to their low surface roughness, narrow pore size distribution (PSD), and low resistance to gas permeation [17,18]. However, while they ensure adequate surface quality for thin layer deposition, ceramic supports prove to be fragile when introduced in the reactor environment. Particularly difficult is their connection and sealing to the steel parts of most reactors structures, making them prone to breakage and/or leaks and thus rendering the scale-up of membrane modules a difficult task [19]. For these reasons, a variety of steel and steel alloys supports have gained rising interest as possible substitutes. They in fact do not require sealing (which can be substituted by a simple weld) and are way less prone to breakage or crack formation thanks to their high mechanical stability. Metallic supported Pd films, however, are proved to be inclined to atomic migration within the support structure, a phenomenon known as intermetallic diffusion or Pd-support interaction [20,21]. In addition, steel-based supports display in fact large surface roughness, large superficial potholes, and wide pore size distribution, making the preparation of Pd-based membranes with high $H_2$ permeation and selectivity a complex task [22,23]. In order to then acquire metallic supports with the desired characteristics, tailor made supplier treatments and extremely low media grades must be requested, clearly increasing their final costs [24]. In our work, we focus on operating suitable and cost-effective supports pre-treatments while starting from a large media grade, rough and unrefined Hastelloy filter. The focus is on acquiring a low-cost product and operating suitable pre-treatments to achieve a sufficient surface quality for deposition of a selective Pd–Ag layer.

To solve the intermetallic diffusion issue, an additional barrier is required between the Pd layer and the metallic support [25]. Several interdiffusion barriers have in fact been extensively investigated in literature, mostly ceramic based ($Al_2O_3$ [26], ZrO [27,28], CeO [29], $SiO_2$ [30]) or oxidation based (controlled metal oxides growth [31]). In our previous work [24], we proposed a boehmite-based layer with a dual function as interdiffusion barrier/smoothening layer. In fact, this layer, besides preventing intermetallic diffusion, if combined with a suitable polishing treatment is also able to reduce the surface roughness of the selected metallic supports. However, the deposition of this barrier alone proves insufficient to close the large superficial pore mouths of the filter, resulting in membranes with low perm-selectivity [24,26]. For this reason, this work focuses on the recovery of superficial porosity of polished filters via chemical etching [32], and the subsequential pore flow distribution narrowing via the introduction of a pore filler. In literature, several materials have been in fact introduced as fillers in an effort to improve the surface morphology of metallic supports [33–37]. Similarly, in the recent work of Kim et al. a selective membrane obtained via pore filling method and sol-gel barrier deposition has been tested for ammonia decomposition applications [38].

In our work, we propose asymmetrically layered $\alpha$-$Al_2O_3$ inside the filter's superficial pore mouths. The sequential filling is carried out with $\alpha$-Al2O3 of decreasing particle size via vacuum assisted aspiration. The surface roughness of the support is then lowered by the deposition of the boehmite-based barrier, covering the pores and preventing interdiffusion issues. The filling effect was studied by feeding imaging parameters to a Two-way ANOVA design, introducing an applicable method for statistical evaluation of membrane

preparation parameters. The outcomes in terms of support gas permeance, pore flow distribution, surface roughness and morphology are thoroughly investigated for each pre-treatment step and, finally, the electroless deposition of a Pd–Ag layer is performed. The resulting membranes are then characterized in terms of ideal $H_2/N_2$ perm-selectivity.

## Experimental

### *Preparation of porous Hastelloy X supports*

Commercial unrefined porous Hastelloy X filters with an outer diameter of 1.2 cm, average surface roughness (Ra) of 6.1 μm, and 0.5 μm nominal media grade (MG) were acquired by Hebei Golden Flame Wire Mesh Co, China. The supports are cut in samples of 10 cm length and welded to dense stainless steel (AISI316L) tubes, in order to achieve a one close end configuration. To preliminarily reduce the surface roughness of the filters, the sample supports were polished in an industrial surface finishing machine via wet-polishing mechanism (ERBA EVT-170). The chosen polishing time amounts to 6 h, as it allows for a suitable trade-off between surface roughness reduction and gas permeation preservation, which was determined in our previous work [24]. The polished supports are then etched by perpendicular immersion in aqua regia for 30 s and thoroughly rinsed with deionized water to remove all mordant residuals. The supports are then oxidized for 1 h at 750 °C in a furnace in static air atmosphere. Before further treatments, the supports are further rinsed both in ethanol and in deionized water in an ultrasonic bath, to remove all impurities resulting from the preparation pre-treatments and handling.

### *Filler introduction*

The tubular supports are submerged in a powder-water suspension, which is pulled through the superficial pores via vacuum assisted dip-coating. The immersion time is set to 60 s per cycle. Between each cycle the support is gently rinsed with distilled water, and no calcination is required. The selected filler powder is $\alpha$-$Al_2O_3$, which is evaluated in three different particle sizes (AA-1 Sumitomo 1 μm, AA-5 Sumitomo 5 μm, AA-20 Sumitomo 18 μm). The powders are 10 wt% suspended in water with a magnetic stirrer. The suspension is improved by addition of $HNO_3$ (67%vol) dropwise. First, the supports undergo several immersion cycles in order to assess both the aspiration effect and the filler size effect on support's PSD and surface morphology. In a second study, supports are filled asymmetrically with $\alpha$- $Al_2O_3$ of decreasing particle size.

### *Interdiffusion layer deposition*

A smoothening interdiffusion barrier is deposited to finalize the improvement of support's surface roughness and ease Pd–Ag deposition. Solutions with boehmite loading 0,9 wt% are prepared in distilled water, incorporating a water-based solution of organic additives, namely 3.5 wt% polyvinyl alcohol (PVA) (MW 130000) and 1 wt% polyethylene glycol (PEG) (MW 400). The deposited layers are dried under rotation in a climate chamber at 40 °C and 60% relative humidity for 1 h. The layers are then sintered for 1 h at 550 °C in a static air furnace. These parameters yield to a mesoporous $\gamma$-$Al_2O_3$ layer about 540 nm thick [24].

### *Pd–Ag deposition*

A layer of Pd–Ag alloy is deposited onto treated supports via electroless plating technique, reported in a previous work by Tanaka et al. [13,14]. To improve membrane selectivity, a consecutive plating procedure is carried out to achieve thicker Pd–Ag layers. After each plating step, the membrane is annealed at 550 °C in 10 vol% $H_2$ - 90 vol% Ar atmosphere for 4 h. At temperatures below 300 °C, only Ar was used to avoid fragilization of the Pd–Ag layer.

### *Characterizations*

#### *Capillary flow porometry*

To evaluate pore size distribution (PSD) variations for each support pre-treatment, the capillary flow porometry technique (CFP, or gas-liquid displacement method) is employed. This technique relies on imposing a *trans*-sample pressure at which a suitable liquid is displaced from the pores of the examined sample. The displacement is detected by registering the permeating flow of a non-reactive gas through the media. In CFP tests, the sample is filled with a wetting liquid, assuming the filling of its entire accessible porosity. Pressure is applied to one side, while the other is kept at atmospheric pressure. This *trans*-sample pressure difference forces the wetting liquid out of the pores resulting in a permeating flow. Increasing the *trans*-sample pressure will promote pore clearance, increasing the permeating flow until the sample is fully cleared from the wetting liquid. Young-Laplace equation is then used to correlate the capillary pressure in the media with its pore diameter. If the capillary is assumed of cylindrical shape, Washburn equation can be applied, which is a typical assumption for indirect method CFP measurements [39,40]:

$$d = -\frac{4\gamma \cos \vartheta}{\Delta P}$$

where ΔP is the applied *trans*-sample pressure, d is the narrowest diameter of the capillary, $\gamma$ is the surface tension of the chosen wetting liquid, and $\vartheta$ is the contact angle between the wetting liquid and the wet surface. The 10 cm porous tubes are measured via CFP technique in a geometry-specific setup (Fig. 1), which consists of.

A. a tubular permeation box, which is able to withstand pressures up to 60 bara;
B. An automatic mass flow controller for $N_2$ (Bronkhorst EL-FLOW Select F-221 M), which is chosen as inert displacement gas;

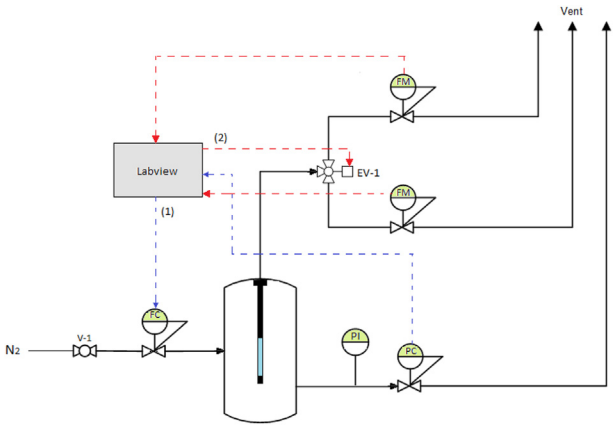


**Fig. 1 – Graphical representation of the CFP setup for tubular membrane samples.**

C. An automatic backpressure regulator at the retentate side (Bronkorst EL-PRESS- P–502C);
D. An automatic three way valve, which can switch between a low flow automatic flowmeter (Bronkhorst EL-FLOW Prestige FG-111B, range 0.004 ml/min - 0.2 l/min) and a high flow automatic flowmeter (Bronkhorst EL-FLOW Prestige FG-111B range 0.2 l/min-10 l/min);
E. An external computer with LabVIEW software.

The setup is fully automated as it follows.

I. The controlling software allows the user to set a desired pressure ramp and/or step to be imposed within the permeation box;
II. The correct feed flow is sent to the permeation box in order to increase the pressure according to the ramp set by the user (1);
III. The permeating flow at each timestamp is registered at the permeate side by the flowmeter with the correct flow range, which can be automatically switched via the three way valve (2).

*Laser confocal microscopy and profilometry: statistical approach*

The surface morphology of the treated filters was studied using a dual optical-3D laser confocal microscope (VKX-3000, Keyence, Osaka, Japan). Said imaging method has been employed to verify and observe the presence of the selected filling particles into the superficial pore mouths of the supports. The extent of superficial pore filling is evaluated by imaging a superficial pore mouth and registering its highest point on the metal surface and its lowest point on the embedded filler. For each filler size and cycles combination, 10 random pore mouths have been evaluated. The result is a filling extent parameter Δ. Consequentially, a lower Δ indicates a fuller pore mouth.

Δ has been employed for statistical considerations as dependent variable in a two-way ANalysis Of VAriance (ANOVA), in order to guarantee a more quantitative approach to the filling procedure optimization [41]. The average surface roughness (Ra) and average profile height (Rz) of the treated supports are evaluated with a portable contact profilometer (MarSurf PS 10) on 10 random positions on the tubular support. These parameters are normalized on their values for an untreated support and employed as dependent variables for a two-way ANOVA.

Being an inferential statistics method, ANOVA allows to infer on the whole population of support pores, while observing only a representative sample amount. The factorial design allows for full observation of the outcome variable (Δ, Ra, or Rz) while variating the two selected factors "Filling cycles" and "Filler size" combinations, making it especially suitable for a comprehensive observation of the filling phenomena.

The experimental designs are summed up in Table 1 and the full statistical documentation is attached in the supplementary material to this manuscript.

*Gas permeance*

The prepared Pd–Ag membranes are tested for $N_2$ permeance at 20 °C and 1 bar in a permeation box, described in our previous work [24]. If the $N_2$ permeance is lower than $1 \cdot 10^{-9}$ mol/m$^2$/s/Pa the membrane is selected for further high temperature short-term investigation. The selected membranes are activated at 400 °C with an air flow of 1 l/min for 2 min. They are then tested at 400, 450 and 500 °C for single-gas $H_2$ and $N_2$ permeance with an imposed pressure difference of 1, 2, 3 bar.

## Results and discussion

### *Polishing and etching*

The evolution of the filters surface with the chosen pre-deposition treatments is analyzed with the laser confocal microscopy images in Fig. 2. The untreated 0.5 μm media grade filters are characterized by the presence of high profile peaks (red) and large surface roughness (Fig. 2a), in agreement with the behavior observed in our previous studies [24]. At this stage, the pore mouths of the support are interconnected, showing a superficial diameter larger than 50 μm. After 6 h of polishing (Fig. 2b), the surface of the support is uniformly smoothened, erasing the presence of the large peaks by plastic deformation. However, the smaller superficial openings are mostly erased. A few large, isolated pore mouths remain, with superficial diameters close to 20 μm. After etching the support for 30s in aqua regia (Fig. 2c) the smoothened surface is broken down into smaller channels interconnecting the metallographic structure underneath: the surface roughness reduction achieved by polishing is preserved, while the support's valleys are uncovered. This promotes an increase in the number of superficial openings, leading to improved gas permeance after polishing, while preserving the treatment's smoothening effect. The evolution of $N_2$ permeance, mean flow pore and contact roughness parameters (Table 2) further confirms the behavior observed via microscopy. Firstly, the polishing treatment promotes both a gas permeance reduction of 76%, and a roughness decrease of 87%. Following the chemical etching, due to the presence of a larger amount of profile valleys, Ra is re-increased solely with an additional

**Table 1 – Two-way ANOVA design for each dependent variable Δ, Ra, Rz.**

| Laser-confocal microscopy | | | |
|---|---|---|---|
| **Definition** | **Variable type** | **Name** | **Variable levels** |
| Outcome | Dependent | Δ [μm] | – |
| Factor 1 | Independent (A) | Filling cycles [–] | 10, 15, 20 |
| Factor 2 | Independent (B) | Filler size [μm] | 1.5, 5, 18 |
| **Average surface roughness (Ra)** | | | |
| **Definition** | **Variable type** | **Name** | **Variable levels** |
| Outcome | Dependent | Ra [μm] | – |
| Factor 1 | Independent (A) | Filling cycles [–] | 10, 15, 20 |
| Factor 2 | Independent (B) | Filler size [μm] | 1.5, 5, 18 |
| **Average profile height (Rz)** | | | |
| **Definition** | **Variable type** | **Name** | **Variable levels** |
| Outcome | Dependent | Rz [μm] | – |
| Factor 1 | Independent (A) | Filling cycles [–] | 10, 15, 20 |
| Factor 2 | Independent (B) | Filler size [μm] | 1.5, 5, 18 |

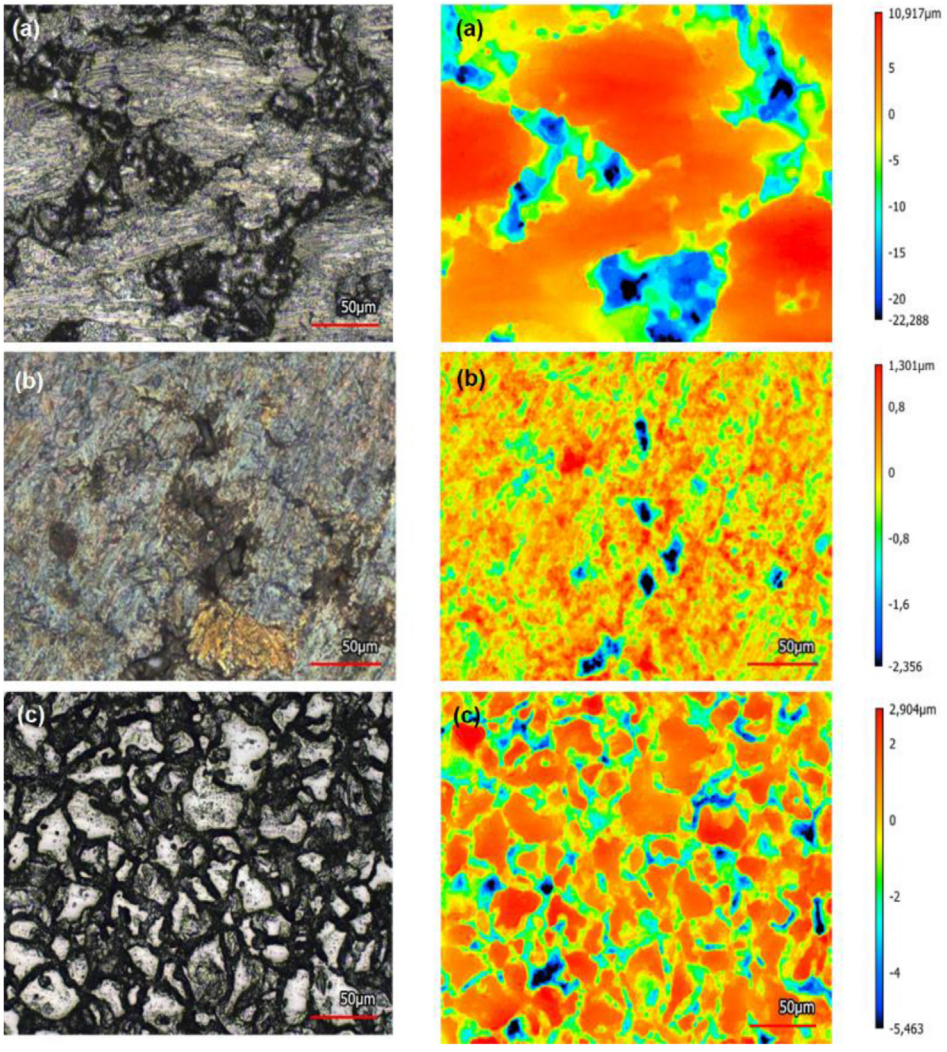


**Fig. 2 – Laser confocal microscopy imaging and height distribution of a 0.5 μm media grade Hastelloy filter (a)untreated (b) 6 h polished, (c) Etched 30s in aqua regia.**

**Table 2 – Ra, $N_2$ permeance, and CFP measured mean flow pore of a sample Hastelloy support for each pre-treating step, compared with the values for an untreated Hastelloy filter and an $\alpha$-$Al_2O_3$ support by Rauschert.**

| Pre-treatment | Ra | $N_2$ permeance | Mean flow pore (CFP) |
|---|---|---|---|
| [–] | [μm] | [mol/s/m$^2$/Pa ·10$^{-5}$] | [μm] |
| Ceramic, $\alpha$-$Al_2O_3$ | 0,5 | 8,0 | 0,1 |
| Untreated Hastelloy | 6,1 | 5,0 | 1,8 |
| Wet polishing, 6 h | 0,8 | 1,2 | 1,9 |
| Chemical etching, 30s | 1,1 | 8,9 | 1,1 |

20%, while the gas permeance surpasses the untreated support's original value. This behavior is well in agreement with the work of Xu et al. which carried out similar improving pre-treatments on a disk-shaped stainless steel support, observing the same surface variations via Scanning Electron Microscopy [32].

*Filler introduction*

Taking into account the mean flow pore of a ceramic support (Table 2), which is proved to produce supported thin and ultra-thin Pd based membranes without defects [42,43], the size of the filter's through pores after polishing and etching is still too large. For this reason, the introduction of the $\alpha$-$Al_2O_3$ filler into the superficial openings of the pre-treated support is expected to prove crucial for the reduction of their size, ensuring gas tightness (and therefore $H_2$ selectivity) of the completed membrane. Table 3 shows the results of the Two-way ANOVA performed on the outcome variables listed in Table 1.

The results of the two-way ANOVA highlight a statistically significant contribution to Δ of the interaction between the number of aspiration cycles and the filler size. When an interaction is statistically significant, analyzing solely the main effects can be misleading. Therefore, the interaction effect is observed in Fig. 3. In particular, all filler sizes underperform with the lowest number of cycles, meaning that more

**Table 3 – ANOVA test results on outcome variables Ra, Rz and Δ. The relevant factor effect is assumed significant if p-value<0.05, with a confidence interval of 95%.**

| Laser confocal microscopy, Δ | | | |
|---|---|---|---|
| Factor | Factor levels | p-value | Significance |
| Filling cycles [–] | 10/15/20 | 0,581 | – |
| Filler size [μm] | 1,5/5/18 | $2{,}3\cdot10^{-8}$ | *** |
| Interaction [-,μm] | – | 0,002 | ** |
| **Profilometry, Ra** | | | |
| Factor | Factor levels | p-value | Significance |
| Filling cycles [–] | 10/15/20 | 0,001 | ** |
| Filler size [μm] | 1,5/5/18 | 0,123 | – |
| Interaction [-,μm] | – | 0,512 | – |
| **Profilometry, Rz** | | | |
| Factor | Factor levels | p-value | Significance |
| Filling cycles [–] | 10/15/20 | 0,001 | *** |
| Filler size [μm] | 1,5/5/18 | 0,025 | * |
| Interaction [-,μm] | – | 0,782 | – |

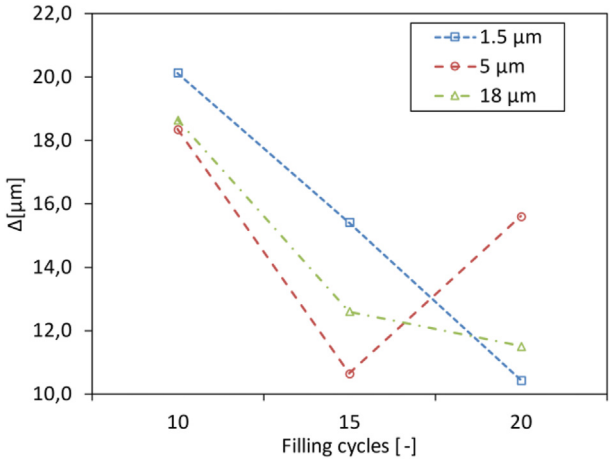


**Fig. 3 – Interaction effect plot of dependent variable Δ against factor "Filling cycles", grouped by "Filler size". The points indicate the average value for each factor levels combination.**

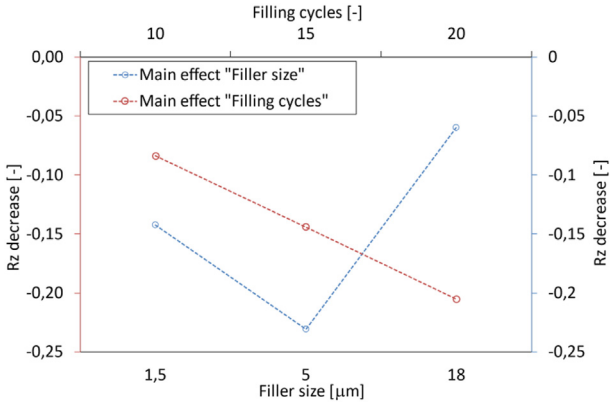


**Fig. 4 – Main independent effects plots of factor "Filling cycles" and factor "Filler size" on dependent variable Rz. The points indicate the average Rz decrease values for each independent factor level.**

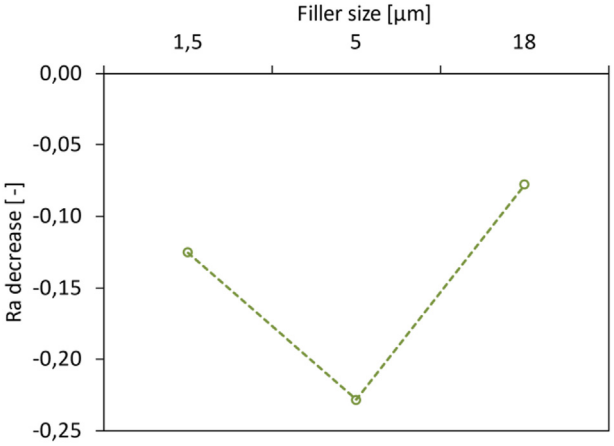


**Fig. 5 – Sole main effect plot of factor "Filler size" on dependent variable Ra. The points indicate average Ra decrease for each level of the sole factor "Filler size".**

than 10 cycles are required for a low Δ; at 15 cycles, the best performing size is 5 μm, while at 20 cycles the largest size (18 μm) and the smallest size (1.5 μm) also contribute to a Δ reduction. This result suggests that 5 μm is a filler that most suits the shape of the superficial pore mouths of the support, requiring less cycles to reach a performance plateau with respect to the largest and smaller filler, which will require more cycles. This result is confirmed by the ANOVA performed on the roughness parameter Rz. For Rz a statistically significant contribution of both independent factors is observed, while the interaction effect is lost. This can be explained by the nature of the outcome variable Rz, which averages roughness profile extremes along a measuring length, rather than purposefully imaged pore mouths, yielding to a loss of information with respect to microscopy. Nevertheless, in Fig. 4b it is noticeable how a 5 μm filler promotes the largest reduction in Rz, independently from the number of cycles performed. However, a large number of

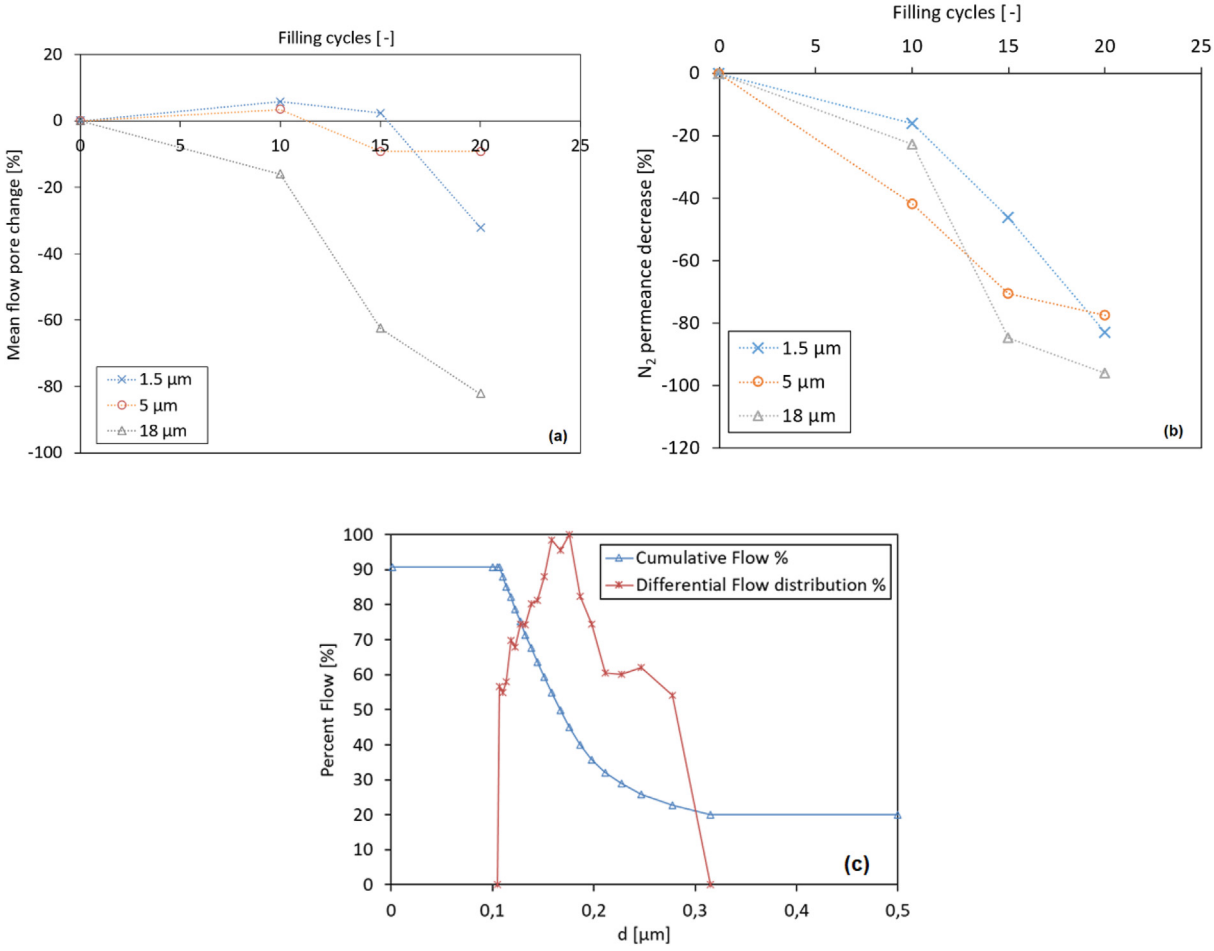


**Fig. 6 – (a)Mean flow pore diameter precent decrease with increasing filling cycles, for each filler size, measured via CFP. (b) $N_2$ permeance percentage decrease with increasing filling cycles, for each filler size. (c) Pore flow distribution measured via CFP of a filter filled 20x with 18 μm α-$Al_2O_3$, measured via CFP between 10% and 90% of total dry flow.**

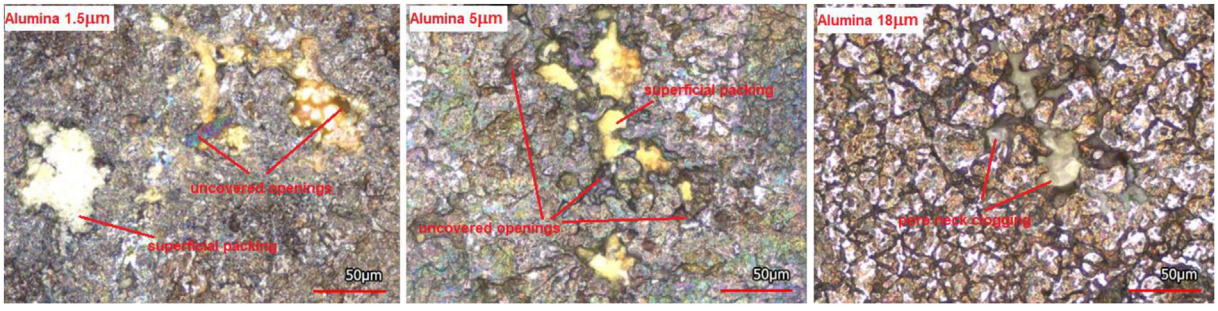


**Fig. 7 – Dual optical-laser confocal imaging of a Hastelloy filter's selected pore mouth filled with 1.5 μm α-$Al_2O_3$, 5 μm α-$Al_2O_3$, and 18 μm α-$Al_2O_3$.**

cycles is preferred independently from the chosen filler size (Fig. 4b). For Ra, a further loss of information is introduced within the ANOVA results. This loss is attributed to the averaging nature of Ra, which does not consider any extremes of the roughness profile, but rather averages all the deviations from the profile's mean line. A statistically significant contribution is attributed solely to the filler size, highlighting how 5 μm is the best performing in terms of Ra reduction independently from the number of applied cycles, which, in turn, proves to be insignificant (Fig. 5).

All three analyses conclude that 5 μm reaches a performance plateau quicker than the other sizes, making it the most suitable size for all surface morphology parameters improvement, preferably in combination with an amount of aspiration cycles greater than 15. However, microscopically, as the number of cycles grows larger, the 1.5 and 18 μm size will contribute to the improving of the pore morphology.

The evolution of surface morphology parameters is not the only phenomenon to be considered while applying a filler to the selected support. An optimal filler design should in fact guarantee sufficient support's average pore diameter reduction and pore distribution sharpening, while preserving gas permeance through the porous media.

From Fig. 6c it is clear how an 18 μm filler sharpens the filter's pore flow distribution around an average pore diameter of about 200 nm, promoting a reduction of the mean flow pore by 80% (Fig. 6a). This shows the filler ability to place itself in large pore necks with respect to the smaller sizes, which only contribute to morphology improvement but require more packing to influence the PSD. Similarly, as observed in Fig. 6b, the 18 μm filler is the most influential in the decrease of permeance in the sample filter, meaning it is affecting the pore necks rather than the surface openings. This conclusion is further confirmed by the dual optical-laser confocal imaging in Fig. 7, in which the 18 μm filler is observed to close the largest defects, while the smaller fillers tend to assume a packed configuration, leaving larger defects open. This renders the 18 μm filler suitable for a first reduction in large support's openings, while fillers of smaller size can be layered to promote a subsequential improvement of the superficial pore morphology. These observations, paired with the results obtained by Chi et al. who observed the same behavior for α-$Al_2O_3$ fillers on lower media grade stainless steel tubes, allow to speculate that fillers with about half of the size of the superficial pore openings are the most suitable for pore flow distribution modification, while fillers of lower dimensions can be used for surface morphology improvement [35].

For this reason, the 18 μm filler is selected as base for the asymmetric support. To then improve the morphology of the support's surface, a 5 μm and 1.5 μm filler are introduced subsequentially. The microscopy in Fig. 8 clearly highlights the presence of large α-$Al_2O_3$ filler underneath the smaller particles, promoting uniform leveling of the pore mouths. Fig. 9 shows the cumulative flow distribution through the pores of a sample filter filled with the selected asymmetric design. The mean flow pore is sufficiently reduced around 100 nm, a comparable value to the one of the α-$Al_2O_3$ supports commonly used in ceramic membranes preparation. At this stage, most of the largest pore necks are reduced in size by the fillers. However, about 10% of the inert gas flow is still measured through pores larger than 500 nm. This pore distribution tail depends on both the initial filters themselves and any leftover large openings after pre-treatment. The control of this tail, although representing the minority of the distribution, proves in fact crucial to minimize membrane's $N_2$ permeation and thus selectivity, ensuring reproducibility of performance. For this reason, further optimization on the filling procedure is the subject of planned studies.

### *Pd–Ag deposition*

In Fig. 10a the surface morphology of a membrane obtained via deposition of Pd–Ag when carried out on a 0.5 μm media grade filter solely treated with the boehmite based smoothening layer is shown. The boehmite based layer allows for uniform metal deposition on the support's surface. However, the sole presence of this layer is not enough to promote full pore closure and obtain a defect-free Pd membrane. In Fig. 10b the same deposition is carried out on a support in which a 5 μm α-$Al_2O_3$ filler has been introduced. The leveling of the pore surface promoted by the filling of the large support's mouths allows for the Pd–Ag to fully close the superficial openings, obtaining the desired defect-free dense layer even on the large superficial pore mouths. For this reason, the

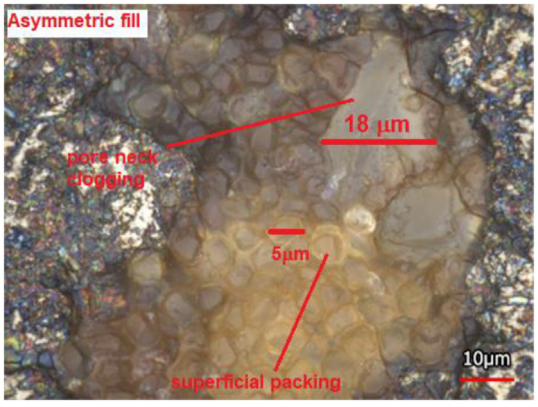


**Fig. 8 – Dual optical-laser confocal imaging of a Hastelloy filter's selected pore mouth, asymmetrically filled with α-$Al_2O_3$ of decreasing size.**

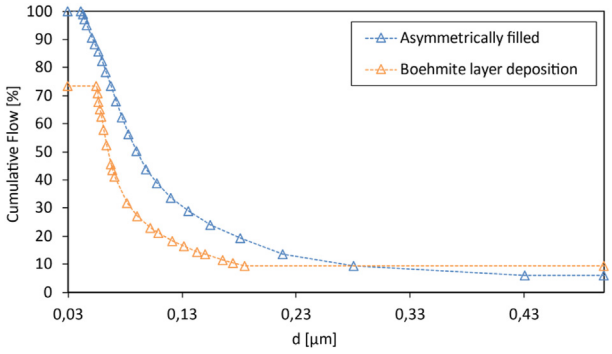


**Fig. 9 – Cumulative percentage flow distribution through the pores of an asymmetrically filled sample filter before and after boehmite layer deposition, measured via CFP.**

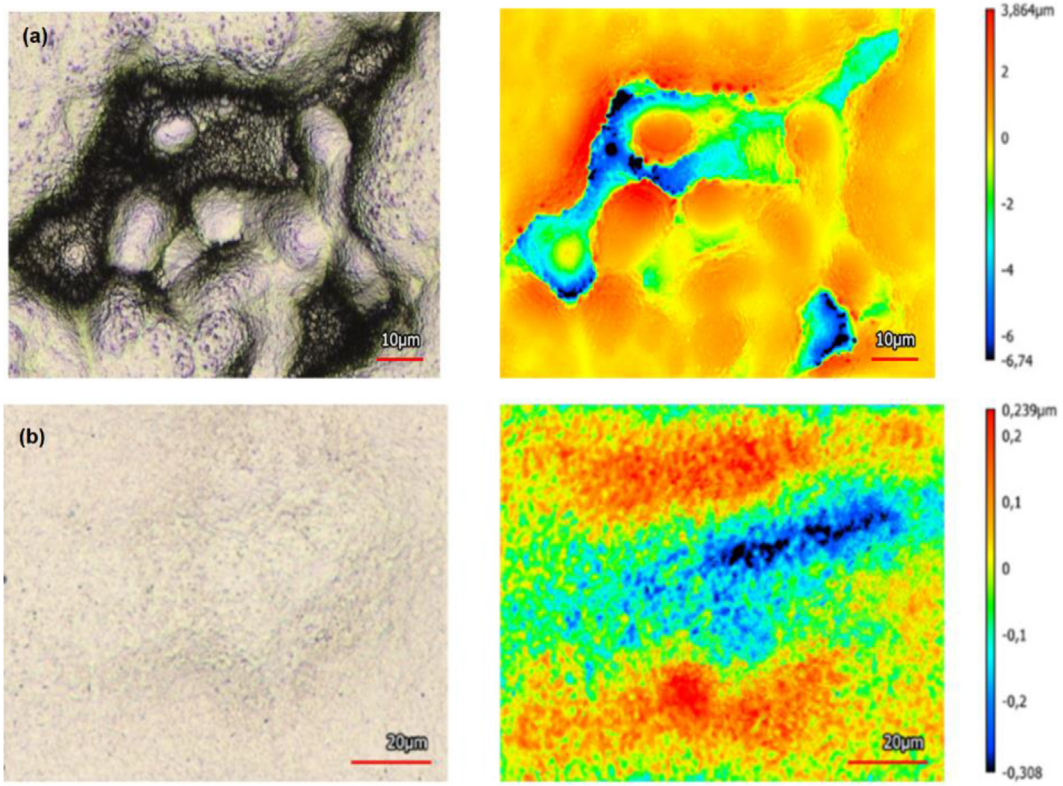


**Fig. 10 – Dual optical-laser confocal imaging and height distribution of a Pd–Ag layer deposited on a large superficial opening of (a) an unfilled Hastelloy filter, (b) a Hastelloy filter filled with $\alpha$-$Al_2O_3$. Both samples are coated with a boehmite-based smoothening layer.**

**Table 4 – $H_2/N_2$ perm-selectivity comparison of Pd-based membranes deposited via electroless plating onto steel-based supports pre-treated with similar methods.**

| Support Material/media grade/pre-treatment | Filler Material/particle size | Interdiffusion barrier Material | $H_2$ permeance [mol/m²/Pa/s] | $H_2/N_2$ [–] | Ref |
|---|---|---|---|---|---|
| Hastelloy X/0.1 µm/pre-treated by Mott Corp. | $Al_2O_3$+YSZ powder/– | No additional layer | $1{,}0\cdot10^{-6}$ | 200 000 | [34] |
| Ceramic/–/double skin | –/– | – | $4{,}6\cdot10^{-6}$ | 26 000 | [12] |
| Inconel 600/–/– | YSZ powder + boehmite -based sol/– | Blow coated YSZ | $3{,}4\cdot10^{-6}$ | 8050 | [38] |
| PSS/0.2 µm/– | CeO/1–4 µm | No additional layer | $1{,}2\cdot10^{-6}$ | infinite | [44] |
| PSS/0.5 µm/polished and etched in alkaline sol and HCl | –/– | none | $5{,}0\cdot10^{-7}$ | 5000 | [45] |
| Inconel 600/0.5 µm/– | YSZ/50 nm | Blow coated YSZ | $7{,}4\cdot10^{-7}$ | 335 | [46] |
| PSS/–/– | YSZ/50 nm | Blow coated YSZ | $3{,}0\cdot10^{-6}$ | 240 | [47] |
| Hastelloy X/0.5 µm/6 h polish | –/– | Boehmite | $2{,}0\cdot10^{-7}$ | 512 | [24] |
| Hastelloy X/0.5 µm/6 h polish, 30s aqua regia etch | $\alpha$-$Al_2O_3$/300 nm | boehmite-based layer 1.2 wt% | $1{,}1\cdot10^{-6}$ | ~6300 | #MS, This work |
| Hastelloy X/0.5 µm/6 h polish, 30s aqua regia etch | $\alpha$-$Al_2O_3$/300 nm | boehmite-based layer 1.2 wt% | $1{,}1\cdot10^{-6}$ | ~830 | #MS2 This work |
| Hastelloy X/0.5 µm/6 h polish, 30s aqua regia etch | $\alpha$-$Al_2O_3$/300 nm | boehmite-based layer 1.2 wt% | $9{,}2\cdot10^{-7}$ | ~3600 | #MS3 This work |
| Hastelloy X/0.5 µm/6 h polish, 30s aqua regia etch | $\alpha$-$Al_2O_3$/18 µm + 5 µm +1.5 µm | boehmite-based layer 0.9 wt% | $7{,}0\cdot10^{-7}$ | ~43 200 | #MA, This work |

choice of a suitable filling procedure proves essential to impact final membrane performance and reproducibility. In Table 4 membranes prepared with different filling procedures are compared in terms of perm-selectivity at 400 °C (see Fig. 11).

Pd–Ag membranes prepared with a small size filler present poor selectivity compared to the membrane prepared with the asymmetric design. In particular, symmetrically filled membrane #MS has been selected due to its high $H_2/N_2$ selectivity, and its performance is compared to #MAS, prepared on a support filled asymmetrically. Both membranes have been characterized in terms of activation energy via linear regression through the Arrhenius plot in Fig. 12, where #MS shows an activation energy of ~6 kJ·mol$^{-1}$and #MA of 9,3 kJ mol$^{-1}$. While #MA is well in agreement with the activation energy range for thin Pd layer membranes, #MS has a lower value, possibly explained by the presence of scattered larger defects. This deduction is confirmed by the n-values of each membrane, amounting to 0,71 and 0,51, respectively. #MA rate determining step for hydrogen transport is given by the Pd layer, while for #MS the value suggests an influence of the metallic support [34].

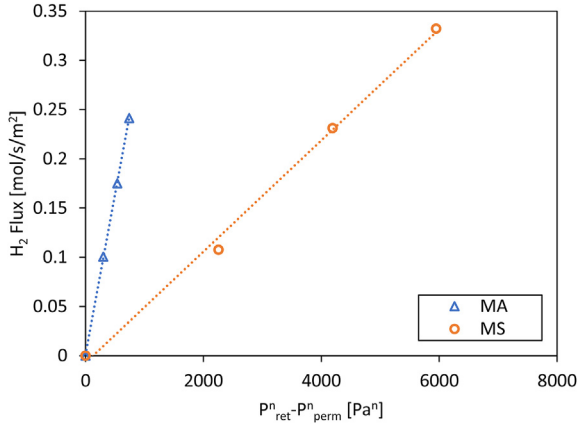


**Fig. 11 – $H_2$ permeating flux vs $H_2$ partial pressure at 400 °C for #MA and #MS.**

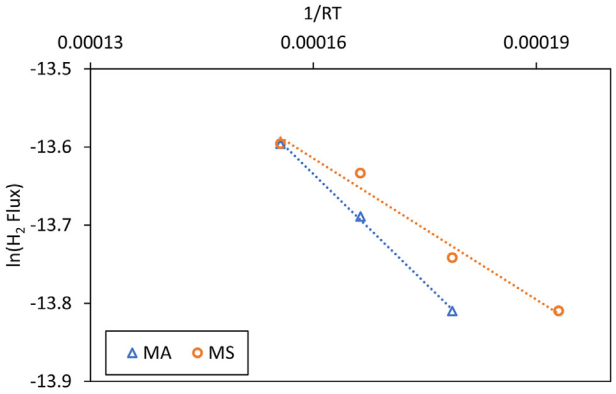


**Fig. 12 – Linear regression performed on Arrhenius plot to determine membrane's activation energy as slope (ΔEa, in J·mol$^{-1}$) and pre-exponential factor as intercept.**

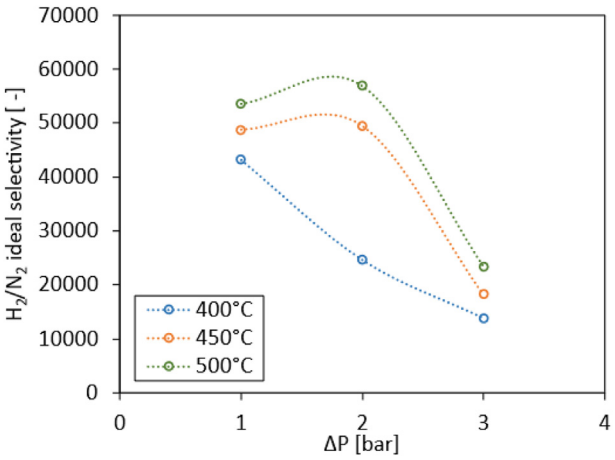


**Fig. 13 – Ideal $H_2/N_2$ selectivity of #MA, measured at 400 °C,450 °C,500 °C with a *trans*-membrane pressure of 1,2,3 bar. The measurements are carried out right after membrane annealing.**

#MA displays an outstanding $H_2/N_2$ selectivity (Fig. 13), accounting that this membrane is prepared on a filter with 0.5 μm media grade and 50 μm large superficial pore mouths, the largest in literature obtaining membranes with selectivity >10000. This result proves that it is indeed possible to achieve high-performing membranes using unrefined metallic filters. Pd–Ag membranes prepared with the same filler aspiration-barrier deposition technique reported in literature show promising performances on steel-based supports with larger media grades (Table 4). This two-step procedure therefore classifies itself as a promising standard method for composite PSS/ceramic/Pd based membranes on cheaper support options.

## Conclusion

Hastelloy porous filters with large media grade (0.5 μm), 2 μm mean flow pore, 50 μm superficial pore mouths and high surface roughness (6 μm Ra) have been successfully modified to improve their superficial characteristics to be used as support of thin Pd–Ag membranes with high $H_2$ permeation and selectivity. Surface roughness can be preliminarily reduced via wet polishing method, producing a decrease in the porosity and gas permeation which can be reverted by subsequential chemical etching in aqua regia. The wide pore flow distribution of the filters can be reduced for the most part up to 200 nm via introduction of α-$Al_2O_3$ filler particles. The 18 μm filler is the most suitable to reduce the pore size distribution applying at least 20 filling cycles, while fillers of lower size (5 μm, 1.5 μm) prove more suitable for further surface morphology improvement. By combining all the studied pre-treatments, a highly selective membrane (~40000) was obtained on a support filled with α-$Al_2O_3$ particles with decreasing particle size. However, further reproducibility studies are needed to ensure complete elimination of leftover unfilled pore mouths on the support filters.

## Declaration of competing interest

The authors declare that they have no known competing financial interests or personal relationships that could have appeared to influence the work reported in this paper.

## Acknowledgements

This project has received funding from the European Union's Horizon 2020 Research and Innovation Programme under grant agreement No 869896 (MACBETH).

## Appendix A. Supplementary data

Supplementary data to this article can be found online at https://doi.org/10.1016/j.ijhydene.2023.03.306.

## REFERENCES

[1] Fernandez E, et al. Palladium based membranes and membrane reactors for hydrogen production and purification: an overview of research activities at Tecnalia and TU/e. Int J Hydrogen Energy 2017;42(19):13763–76. https://doi.org/10.1016/j.ijhydene.2017.03.067.

[2] Arratibel A, Pacheco Tanaka DA, Slater TJA, Burnett TL, van Sint Annaland M, Gallucci F. Unravelling the transport mechanism of pore-filled membranes for hydrogen separation. Sep Purif Technol 2018;203(April):41–7. https://doi.org/10.1016/j.seppur.2018.04.016.

[3] Park J, Bennett T, Schwarzmann J, Cohen SA. Permeation of hydrogen through palladium. J Nucl Mater 1995;220(2):827–31. https://doi.org/10.1016/0022-3115(94)00591-5. –222.

[4] Jokar SM, et al. The recent areas of applicability of palladium based membrane technologies for hydrogen production from methane and natural gas: a review. Int J Hydrogen Energy Feb. 2023;48(16):6451–76. https://doi.org/10.1016/J.IJHYDENE.2022.05.296.

[5] Gallucci F, Fernandez E, Corengia P, van Sint Annaland M. Recent advances on membranes and membrane reactors for hydrogen production. Chem Eng Sci 2013;92:40–66. https://doi.org/10.1016/j.ces.2013.01.008.

[6] Bernardo G, Araújo T, da Silva Lopes T, Sousa J, Mendes A. Recent advances in membrane technologies for hydrogen purification. Int J Hydrogen Energy 2020;45(12):7313–7338, Mar. https://doi.org/10.1016/J.IJHYDENE.2019.06.162.

[7] Gallucci F, Paturzo L, Basile A. A simulation study of the steam reforming of methane in a dense tubular membrane reactor. Int J Hydrogen Energy 2004;29(6):611–7. https://doi.org/10.1016/j.ijhydene.2003.08.003.

[8] Patil CS, van Sint Annaland M, Kuipers JAM. Fluidised bed membrane reactor for ultrapure hydrogen production via methane steam reforming: experimental demonstration and model validation. Chem Eng Sci 2007;62(11):2989–3007. https://doi.org/10.1016/j.ces.2007.02.022.

[9] Bernardo P, Barbieri G, Drioli E. Evaluation of membrane reactor with hydrogen-selective membrane in methane steam reforming. Chem Eng Sci 2010;65(3):1159–1166, Feb. https://doi.org/10.1016/J.CES.2009.09.071.

[10] Guo Y, Wu H, Jin Y, Zhou L, Chen Q, Fan X. Deposition of TS-1 zeolite film on palladium membrane for enhancement of membrane stability. Int J Hydrogen Energy Nov. 2017;42(44):27111–21. https://doi.org/10.1016/J.IJHYDENE.2017.09.127.

[11] Arratibel Plazaola A, Pacheco Tanaka DA, Van Sint Annaland M, Gallucci F. Recent advances in Pd-based membranes for membrane reactors. Molecules 2017;22(no. 1). https://doi.org/10.3390/molecules22010051.

[12] Arratibel A, Pacheco Tanaka A, Laso I, van Sint Annaland M, Gallucci F. Development of Pd-based double-skinned membranes for hydrogen production in fluidized bed membrane reactors. J Membr Sci August 2017;550:536–44. https://doi.org/10.1016/j.memsci.2017.10.064. 2018.

[13] Pacheco Tanaka DA, Llosa Tanco MA, Okazaki J, Wakui Y, Mizukami F, Suzuki TM. Preparation of 'pore-fill' type Pd-YSZ-γ-Al2O3 composite membrane supported on α-Al2O3 tube for hydrogen separation. J Membr Sci 2008;320(1–2):436–41. https://doi.org/10.1016/j.memsci.2008.04.044.

[14] Pacheco Tanaka DA, et al. Preparation of palladium and silver alloy membrane on a porous α-alumina tube via simultaneous electroless plating. J Membr Sci 2005;247(1–2):21–7. https://doi.org/10.1016/j.memsci.2004.06.002.

[15] Cechetto V, Di Felice L, Medrano JA, Makhloufi C, Zuniga J, Gallucci F. H2 production via ammonia decomposition in a catalytic membrane reactor. Fuel Process Technol 2021;216:106772. https://doi.org/10.1016/j.fuproc.2021.106772.

[16] Cechetto V, Di Felice L, Gutierrez Martinez R, Arratibel Plazaola A, Gallucci F. Ultra-pure hydrogen production via ammonia decomposition in a catalytic membrane reactor. Int J Hydrogen Energy 2022. https://doi.org/10.1016/j.ijhydene.2022.04.240.

[17] Fernandez E, et al. Development of thin Pd-Ag supported membranes for fluidized bed membrane reactors including WGS related gases. Int J Hydrogen Energy 2015;40(8):3506–19. https://doi.org/10.1016/j.ijhydene.2014.08.074.

[18] Yepes D, Cornaglia LM, Irusta S, Lombardo EA. Different oxides used as diffusion barriers in composite hydrogen permeable membranes. J Membr Sci 2006;274(1–2):92–101. https://doi.org/10.1016/j.memsci.2005.08.003.

[19] de Nooijer N, et al. Long-term stability of thin-film Pd-based supported membranes. Processes 2019;7(2). https://doi.org/10.3390/pr7020106.

[20] Van Dal MJH, Pleumeekers MCLP, Kodentsov AA, Van Loo FJJ. Intrinsic diffusion and Kirkendall effect in Ni-Pd and Fe-Pd solid solutions. Acta Mater 2000;48(2):385–96. https://doi.org/10.1016/S1359-6454(99)00375-4.

[21] Medrano JA, et al. Pd-based metallic supported membranes: high-temperature stability and fluidized bed reactor testing. Int J Hydrogen Energy 2016;41(20):8706–8718, Jun. https://doi.org/10.1016/J.IJHYDENE.2015.10.094.

[22] Tosto E, et al. Stability of pore-plated membranes for hydrogen production in fluidized-bed membrane reactors. Int J Hydrogen Energy 2020;45(12):7374–7385, Mar. https://doi.org/10.1016/J.IJHYDENE.2019.04.285.

[23] Shi Z, Wu S, Szpunar JA, Roshd M. An observation of palladium membrane formation on a porous stainless steel substrate by electroless deposition. J Membr Sci Sep. 2006;280(1–2):705–11. https://doi.org/10.1016/J.MEMSCI.2006.02.026.

[24] Agnolin S, Melendez J, Di Felice L, Gallucci F. ScienceDirect Surface roughness improvement of Hastelloy X tubular filters for H 2 selective supported Pd e Ag alloy membranes preparation. Int J Hydrogen Energy 2022. https://doi.org/10.1016/j.ijhydene.2022.06.164. xxxx.

[25] Nam SE, Lee KH. Hydrogen separation by Pd alloy composite membranes: introduction of diffusion barrier. J Membr Sci Oct. 2001;192(1–2):177–85. https://doi.org/10.1016/S0376-7388(01)00499-9.
[26] Bottino A, et al. Sol-gel synthesis of thin alumina layers on porous stainless steel supports for high temperature palladium membranes. Int J Hydrogen Energy 2014;39(9):4717–24. https://doi.org/10.1016/j.ijhydene.2013.11.096.
[27] Chotirach M, Tantayanon S, Tungasmita S, Kriausakul K. Zr-based intermetallic diffusion barriers for stainless steel supported palladium membranes. J Membr Sci Jul. 2012;405(406):92–103. https://doi.org/10.1016/J.MEMSCI.2012.02.055.
[28] Huang Y, Dittmeyer R. Preparation of thin palladium membranes on a porous support with rough surface. J Membr Sci 2007;302(1–2):160–70. https://doi.org/10.1016/j.memsci.2007.06.040.
[29] Qiao A, et al. Hydrogen separation through palladium–copper membranes on porous stainless steel with sol–gel derived ceria as diffusion barrier. Fuel 2010;89(6):1274–1279, Jun. https://doi.org/10.1016/J.FUEL.2009.12.006.
[30] Katoh M, Ueshima T, Takatani M, Sugiura H, Ominami K, Sugiyama S. Effects of different silica intermediate layers for hydrogen diffusion enhancement of palladium membranes applied to porous stainless steel support. Sci Rep 2020;10(1):1–12. https://doi.org/10.1038/s41598-020-62054-3.
[31] Samingprai S, Tantayanon S, Ma YH. Chromium oxide intermetallic diffusion barrier for palladium membrane supported on porous stainless steel. J Membr Sci Feb. 2010;347(1–2):8–16. https://doi.org/10.1016/J.MEMSCI.2009.09.058.
[32] Xu N, Ryi S, Li A, Grace JR, Lim J, Boyd T. Improved pre-treatment of porous stainless steel substrate for preparation of Pd-based composite membrane. Can J Chem Eng 2013;91(10):1695–701. https://doi.org/10.1002/cjce.21793.
[33] Wei L, Hu X, Yu J, Huang Y. Aluminizing and oxidation treatments on the porous stainless steel substrate for preparation of H2-permeable composite palladium membranes. Int J Hydrogen Energy Oct. 2014;39(32):18618–24. https://doi.org/10.1016/J.IJHYDENE.2014.03.031.
[34] Fernandez E, et al. Preparation and characterization of metallic supported thin Pd–Ag membranes for hydrogen separation. Chem Eng J 2016;305:182–90. https://doi.org/10.1016/j.cej.2015.09.119.
[35] Chi Y-H, Yen P-S, Jeng M-S, Ko S-T, Lee T-C. Preparation of thin Pd membrane on porous stainless steel tubes modified by a two-step method. Int J Hydrogen Energy 2010;35(12):6303–6310, Jun. https://doi.org/10.1016/j.ijhydene.2010.03.066.
[36] Nayebossadri S, Fletcher S, Speight JD, Book D. Hydrogen permeation through porous stainless steel for palladium-based composite porous membranes. J Membr Sci Oct. 2016;515:22–8. https://doi.org/10.1016/J.MEMSCI.2016.05.036.
[37] Zahedi M, Afra B, Dehghani-Mobarake M, Bahmani M. Preparation of a Pd membrane on a WO3 modified Porous Stainless Steel for hydrogen separation. J Membr Sci May 2009;333(1–2):45–9. https://doi.org/10.1016/J.MEMSCI.2009.01.053.
[38] Kim TW, et al. Highly selective Pd composite membrane on porous metal support for high-purity hydrogen production through effective ammonia decomposition. Energy Dec. 2022;260:125209. https://doi.org/10.1016/J.ENERGY.2022.125209.
[39] Tanis-Kanbur MB, Peinador RI, Hu X, Calvo JI, Chew JW. Membrane characterization via evapoporometry (EP) and liquid-liquid displacement porosimetry (LLDP) techniques. J Membr Sci Sep. 2019;586:248–58. https://doi.org/10.1016/J.MEMSCI.2019.05.077.
[40] Li D, Frey MW, Joo YL. Characterization of nanofibrous membranes with capillary flow porometry. J Membr Sci Dec. 2006;286(1–2):104–14. https://doi.org/10.1016/J.MEMSCI.2006.09.020.
[41] Orooji Y, Ghasali E, Emami N, Noorisafa F, Razmjou A. ANOVA design for the optimization of TiO2 coating on polyether sulfone membranes. Molecules 2019;24(16). https://doi.org/10.3390/molecules24162924.
[42] Fernandez E, et al. Development of highly permeable ultra-thin Pd-based supported membranes. Chem Eng J Dec. 2016;305:149–55. https://doi.org/10.1016/J.CEJ.2015.11.060.
[43] Melendez J, Fernandez E, Gallucci F, van Sint Annaland M, Arias PL, Pacheco Tanaka DA. Preparation and characterization of ceramic supported ultra-thin (~1 μm) Pd-Ag membranes. J Membr Sci 2017;528(2017):12–23. https://doi.org/10.1016/j.memsci.2017.01.011.
[44] Tong J, Matsumura Y, Suda H, Haraya K. Thin and dense Pd/CeO2/MPSS composite membrane for hydrogen separation and steam reforming of methane. Sep Purif Technol Nov. 2005;46(1–2):1–10. https://doi.org/10.1016/J.SEPPUR.2005.03.011.
[45] Mardilovich PP, She Y, Ma YH, Rei MH. Defect-free palladium membranes on porous stainless-steel support. AIChE J 1998;44(2):310–22. https://doi.org/10.1002/aic.690440209.
[46] Do HY, Kim CH, Han JY, Kim HS, Ryi SK. Low-temperature proton-exchange membrane fuel cell-grade hydrogen production by membrane reformer equipped with Pd-composite membrane and methanation catalyst on permeation stream. J Membr Sci Sep. 2021;634:119373. https://doi.org/10.1016/J.MEMSCI.2021.119373.
[47] Kim CH, Han JY, Lim H, Lee KY, Ryi SK. Hydrogen production by steam methane reforming in membrane reactor equipped with Pd membrane deposited on NiO/YSZ/NiO multilayer-treated porous stainless steel. J Membr Sci Oct. 2018;563:75–82. https://doi.org/10.1016/J.MEMSCI.2018.05.037.